ACS OMEGA

Open Access

This article is licensed under CC-BY-NC-ND 4.0

http://pubs.acs.org/journal/acsodf

Article

Programmable Twisting of Flexible Nanosurfaces with Attached Chiral Ligands

Pavel L. Rehak, Michal Sawczyk, and Petr Král*

Cite This: *ACS Omega* 2026, 11, 66252−66258

Read Online

ACCESS | Metrics & More | Article Recommendations | Supporting Information

ABSTRACT: Chiral molecules attached to flexible nanoscale surfaces can interact cooperatively and deform their underlying surfaces in complex ways. Here, molecular dynamics simulations are used to model graphene ribbons with covalently attached chiral gluconic acid molecules in different crystal orders. The simulations revealed that asymmetric steric forces acting between the chiral molecules can generate stresses and torques that cause bending and helical twisting of the functionalized nanoribbons depending on their cut direction, relative sizes, ligand density, enantiomeric excess, and overall history. Upon annealing and quenching in water, the ligands can remain in the same crystalline phase, switch to a new phase, or become randomly oriented. Such deformable nanosystems can be implemented in sensing, mimicking, and memory applications.

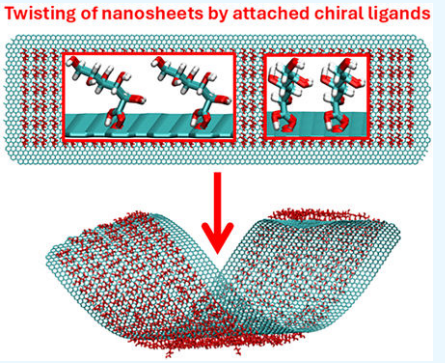

INTRODUCTION

Chirality is ubiquitous across many scales, different phases, and various forms in biological, organic, and inorganic chemistry systems.[1−4] When chiral molecules assemble into superstructures, their asymmetric cooperative molecular-scale interactions can be hierarchically amplified into twisted ribbons, helices, helicoids, and other superstructures[5−8] with a tunable pitch, handedness, and morphology.[9,10] The enantiomeric excess plays a big role, as enantiopure chiral molecules often form twisted low-D structures, while their racemates tend to assemble into centrosymmetric 3D crystals.[11,12]

Adsorption of chiral molecules on inorganic materials can also affect their growth.[13,14] Peptide fibrils adsorbed on graphene can twist it in a helical manner.[15,16] Twisted superstructures can also form in spontaneous symmetry-breaking processes. For example, nanoparticles and nanosheets with achiral ligands can form helicoidal assemblies.[17−19]

In recent years, numerous studies reported the growth of helically twisted gold nanoparticles when chiral molecules were attached to their surfaces.[20−31] The twisted growth was associated with a preferred binding of chiral molecules to different facets, often attached through strong but labile Au−S thiol bonds. Even though these bonds stabilize the surfaces, they limit the ligand exchange and surface rearrangements.[32−34] Therefore, alternative ligands, including chiral amino acids, peptides, sugar derivatives, and carboxylic acids, have been adopted.[35−37]

However, it is not obvious if asymmetric coupling between chiral ligands can cause a helical growth or twisting of nanostructures. One way to better understand these processes is to study molecular chirality-induced helical deformation of flexible nanostructures. Atomically thin graphene offers a model platform for probing this phenomenon since it combines a high in-plane stiffness with a low bending rigidity, allowing it to behave as a laterally robust yet bendable membrane that is sensitive to relatively weak interfacial forces.[38−40]

Here, we examine this idea using atomistic molecular dynamics (MD) simulations of simplified model chiral systems based on graphene nanoribbons covalently functionalized with chiral gluconic acid (GA) molecules. GAs serve as representative sugar-derived chiral ligands that are increasingly employed as dynamic, nonthiol alternatives.[35,41,42]

RESULTS AND DISCUSSION

Model systems are formed by various ribbons extracted from a graphene sheet covered on one side by a covalently attached monolayer of enantiopure gluconic acid (R-GA) molecules (Figure 1). The equilibrated configuration of such a system should depend on the arrangement of the chiral molecules attached to the flexible sheet. Here, as a proof of concept, we pick one arrangement where R-GAs form a rectangular 2D lattice, with (2,2) × (2,0) (horizontal × vertical) shifts (a = 8.43 Å, b = 5.40 Å), and carbonyl oxygens covalently attached

Received: April 23, 2026
Revised: October 4, 2026
Accepted: October 9, 2026
Published: October 21, 2026



ACS Publications

© 2026 The Authors. Published by American Chemical Society

Downloaded from pubs.acs.org/acsodf/article-pdf/11/43/66252/6893534/acsomega.6c04640.pdf by UNIV OF ILLINOIS CHICAGO, Petr Kral on 12 November 2026

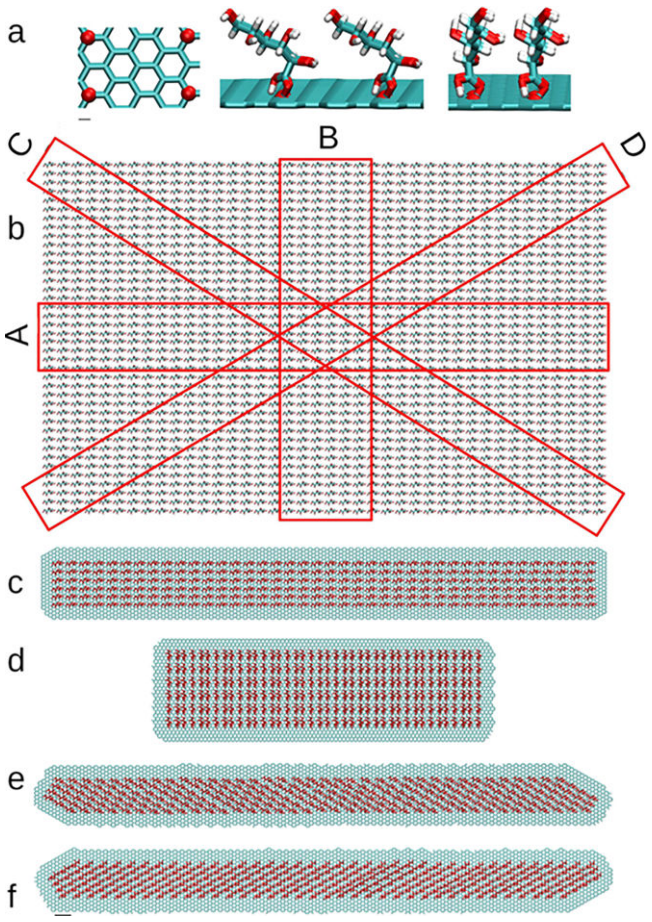

Figure 1. Model graphene ribbons with covalently attached R-GAs. (a) Placement of R-GAs in the (2,2) × (2,0) order on graphene. (b) Graphene sheet where extracted and slightly enlarged ribbons are visualized. (c) Horizontal cut A (40 × 6 R-GAs), (d) vertical cut B (6 × 40 R-GAs), (e) diagonal cut C (231 R-GAs), and (f) diagonal cut D (231 R-GAs). The scale bars are 1 nm long.

to graphene carbons, as shown in Figure 1a (Methods section). For simplicity, we do not include passivating hydrogens at the ribbon edges. The chemistry of this system might not be fully realistic, but it can still serve well for the given purpose of testing. Initially, the axis oriented along the R-GA "C-backbone" was chosen to be tilted about 45° from the axis orthogonal to the sheet in the horizontal direction within the sheet. This choice provides some room for nesting of R-GAs which are covalently attached to the graphene.

We have extracted four model ribbons from the R-GA-functionalized graphene sheet, as shown in Figure 1b. One horizontal (A), one vertical (B), and two diagonal (C, D) model ribbons were extracted and slightly broadened, as shown in Figure 1c–f, respectively. These ribbons were then simulated in water at room temperature. Since the initial simulations revealed that the vertical and horizontal cuts developed opposite helicities, additional cuts at intermediate angles were chosen, which showed a limited helicity, as anticipated. However, given the limited sizes of these ribbons, the parameters of these bending and twisting deformations cannot be precisely determined.

R-GA Ribbons

In the functionalized ribbons, all R-GAs were initially oriented in the same manner (rotational angles about their vertical axis) as discussed above. When the simulations were performed in explicit water at room temperature (T = 310 K and P = 1 atm), this organization of R-GAs was largely maintained because of rotational barriers formed by intermolecular forces.

Figure 2 (left column) shows the (A-D) ribbons simulated for $t \approx 100$ ns at T = 310 K. In all 4 cases, R-GAs reside on the outward side of the bent and helically twisted ribbons, implying their repulsion (steric forces) for the chosen crystal structure. The horizontal (A) and vertical (B) ribbons, where the main R-GAs axes are parallel and tangential to the ribbons, respectively, formed oppositely twisted helices with a radius of $r \approx 3$ nm and pitches of $p \approx 30$ nm and $p \approx 10$ nm. In contrast, the diagonal (C) and (D) ribbons bent along their long axis into cylinders of a $r \approx 3$ nm radius, but their helicity was very small. This could be expected, as these two ribbons are rotated with respect to both the horizontal and vertical ribbons, forming the left and right helices, respectively. At room-temperature simulations (100 ns), only minor defects are seen in the molecular organization of these systems.

Analysis of the Intermolecular Forces

We hypothesize that the graphene ribbons are bent and helically twisted by asymmetric steric and cooperative forces acting between their chiral ligands. To examine these effects, we have extracted from the functionalized ribbon a setup with (3 × 3) R-GA ligands with the same orientations and intermolecular distances, and calculated the intermolecular forces acting between the central ligand and its 8 neighbors (Methods section). At the beginning, as shown in Figure 3, the central R-GA ligand acts on the neighboring R-GA ligands with nonradial forces, giving a net force field with a S_2 (improper C_2) symmetry. Forces originating from the closest 4 ligands are repulsive, and they are larger for ligands that are closer to the central molecule. Each side molecule exerts on the central molecule a force of $F \approx 50-500$ pN, and they all exert on it a total torque of $|M| \approx 40$ kcal/mol. The y component of the torque is dominant, yet it has also significant x and z components. Accumulation of this torque across the functionalized ribbon causes its helical off-plane twisting. During the spontaneous deformation of a functionalized ribbon, the (largely repulsive) forces acting between the ligands are relaxed, while the deformed graphene gains more potential energy. The deformed ribbon likely decreases its overall enthalpy, $\Delta H < 0$. During this spontaneous process, the overall Gibbs free energy of the ribbon should also drop, $\Delta G = \Delta H - T\Delta S < 0$, and reach a local minimum, which might be less affected by entropic contributions.

Later, we study racemic systems with randomly positioned S/R enantiomers. We can qualitatively estimate the effect of these forces in such systems by placing one S(R) enantiomer surrounded by R(S) enantiomers. One such case is shown in Figure S1. It reveals that the forces can still exert torque, but when we add the torques from systems of both symmetries (S within R and R within S), the torques cancel out. This explains why the racemic systems are not twisted but are still bent.

We can draw these observations further and analyze the origin of the ribbon's bending. To do so, we study systems having lower densities of ligands, where ligands are placed at (3,0) and (3,3) instead of (2,0) and (2,2) positions of graphene, shown in Figure S2. At 200 K, the low-density systems have a crystalline arrangement of the ligands, but at room temperature, the molecular organization melts due to weak coupling forces. Figure S2 reveals that the presence of

Downloaded from pubs.acs.org/acsodf/article-pdf/11/43/66252/6893534/acsomega.6c04640.pdf by UNIV OF ILLINOIS CHICAGO, Petr Kral on 12 November 2026

https://doi.org/10.1021/acsomega.6c04640
ACS Omega 2026, 11, 66252−66258

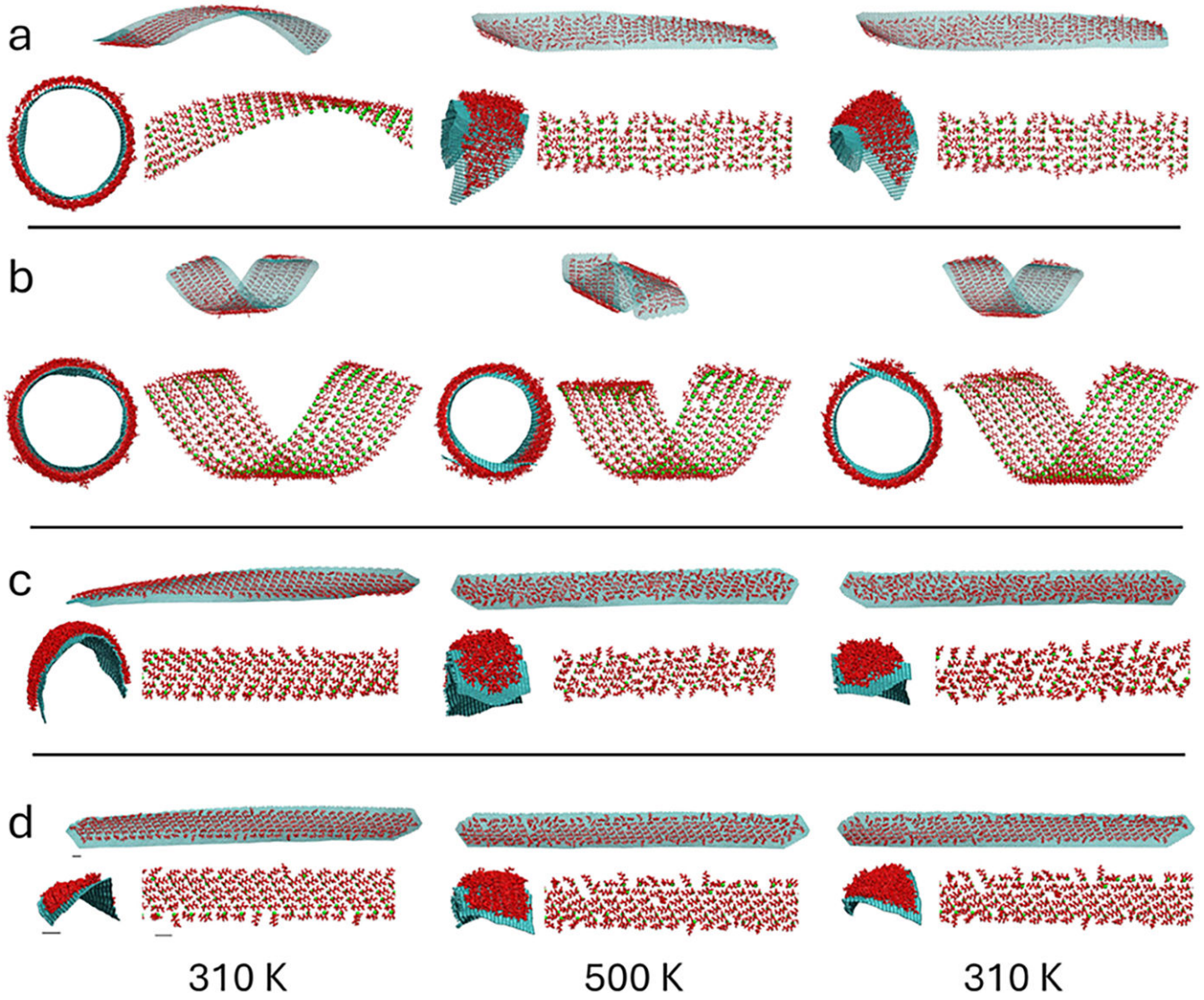

Figure 2. R-GA-covered (A−D) ribbons in (a−d), respectively, initially simulated at 310 K for at least 100 ns (left), then annealed to 500 K for 200 ns, except for A, which was annealed for 300 ns (middle), and finally cooled back to 310 K for 100 ns (right). Each system is represented by a side view of the deformed ribbon, a view along the axis of helical deformation, and molecular details. Scale bars represent 1 nm.

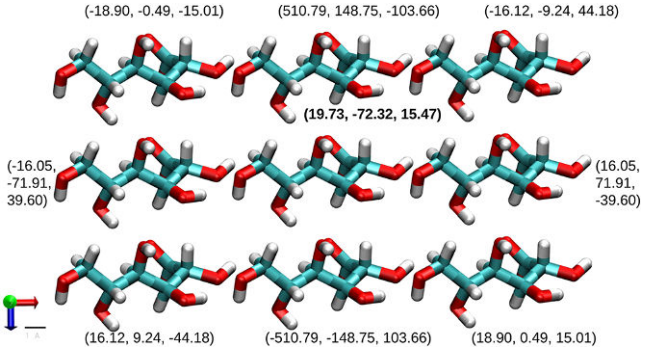

Figure 3. Initial molecular arrangement, forces exerted by the central R-GA molecule on 8 surrounding R-GA molecules, and torque exerted on these 8 molecules obtained for the systems in Figure 2. Forces on the periphery of molecules are presented in pN. The central vector in bold is torque kcal/mol Å. The scale bar represents 1 Å. The *x*, *y*, and *z* directions correspond to (red, green, blue) arrows.

disorder in the molecular orientation can decrease the ribbon helicity. The initial forces, shown in Figure S3, have magnitudes of $F \approx 10-75$ pN. These weak forces are directly responsible for the limited bending and twisting of the ribbon shown in Figure S2. One can extrapolate these observations and conclude that when these steric side forces point, on average, inward (low density of molecules) or outward (high density of molecules) from the central molecule, they cause a concave or convex bending (in 1 or 2 directions) of the ribbons, respectively.

To elucidate the effect of molecular chirality, we have also simulated ribbons covered by achiral hexanonic acid molecules placed regularly on the ribbon surface. As expected, Figure S4 reveals that these ribbons lack any helical twisting at room temperature, but they bend in 2 directions due to steric forces acting between the nearby achiral molecules, shown in Figure S5. At room temperature, the achiral molecules are ordered, but they become more disordered upon annealing at 500 K (see the Discussion section). However, the ribbons look very

Downloaded from pubs.acs.org/acsodf/article-pdf/11/43/66252/6893534/acsomega.6c04640.pdf by UNIV OF ILLINOIS CHICAGO, Petr Kral on 12 November 2026

https://doi.org/10.1021/acsomega.6c04640
ACS Omega 2026, 11, 66252−66258

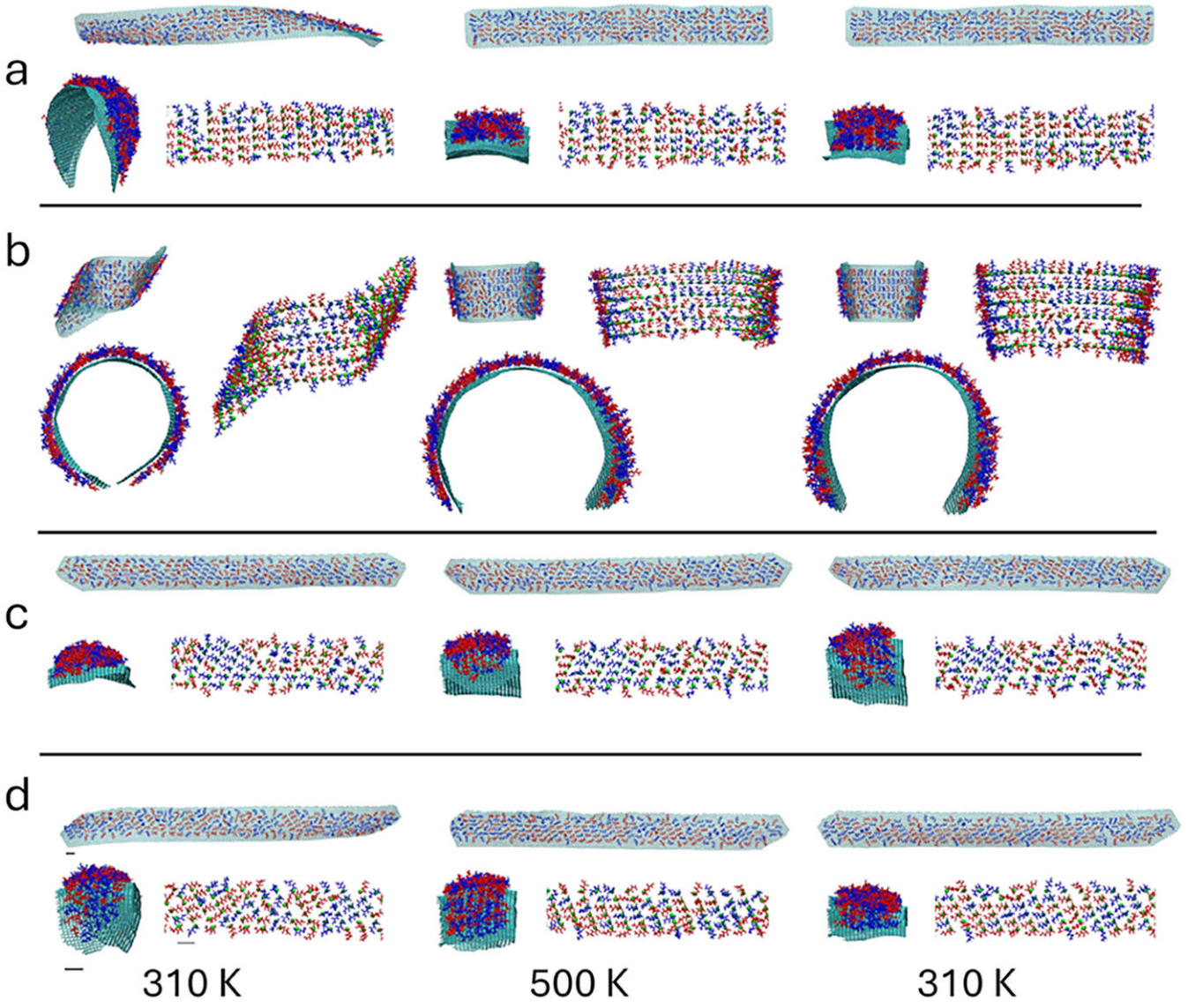

Figure 4. Same as Figure 2, but simulated for ribbons covered with randomly mixed GAs of a 50S-50R composition. (a) Analogous to system A; (b) B; (c) C; (d) D. All systems were initially simulated at 310 K for at least 100 ns (left), then annealed to 500 K for 200 ns (middle), and finally cooled back to 310 K for 100 ns. Blue GA molecules represent S isomer; red GA molecules represent R isomers. Scale bars represent 1 nm.

similar upon annealing. The absence of helicity in these ribbons is caused by the fact that the molecules are achiral.

In all systems, the interligand steric forces predominantly originate from the Lennard-Jones (L-J) coupling (van der Waals attraction and Pauli-like repulsion) and partly from their electrostatic coupling. In the high-density systems, L-J contributions are highly repulsive, while electrostatic contributions might be less relevant. In the low-density systems, L-J contributions are negligibly small and the electrostatic contributions can become more important. The overall deformations of simulated (A-D) ribbons largely agree with the explanations provided above.

Annealing of R-GA Ribbons

The ribbon deformations presented above reveal the presence of steric forces acting between the R-GA molecules. However, the ligands might be kinetically trapped within the chosen crystalline arrangement. Since these forces control the ribbon deformations, disruptions of the crystalline order within the attached R-GAs could affect the ribbon deformations. At elevated temperatures, closely packed and interacting R-GAs could overcome their rotational barriers. To examine this possibility with simulations, we have annealed the functionalized ribbons at T = 500 K for 300 ns and quenched them back at T = 310 K for 100 ns (Methods section), as shown in Figure 2 (left to right).

During the annealing of kinetically trapped systems and their follow-up quenching, both ligands and ribbons might gain new configurations that could decrease their total free energies G. After this procedure, typically, R-GAs became more rotationally disordered when they were initially in less stable local minima. However, in some ribbons, the disorder was rather small, or different crystalline organizations have emerged, as shown in Figure 2. In (A) and (B), the rows of molecules are parallel to the main ribbon axis (attached through green atoms), and their main molecular axes are aligned with the ribbon axis and orthogonal to it, respectively. This mutual orientation of the molecular and ribbon axes can affect the molecular reorganization and ribbon deformation. In (A), R-

Downloaded from pubs.acs.org/acsodf/article-pdf/11/43/66252/6893534/acsomega.6c04640.pdf by UNIV OF ILLINOIS CHICAGO, Petr Kral on 12 November 2026

https://doi.org/10.1021/acsomega.6c04640
ACS Omega 2026, 11, 66252−66258

GAs became significantly rotationally disordered (crystal metastable), which prevented the ribbon from fully retaining its helicity upon cooling, since intermolecular steric forces have lost their chirality-related asymmetry (torque). However, in (B), R-GAs practically did not change their orientations during annealing (crystal stable), so the cold ribbon almost fully recovered its original helical twisting. This could be explained by the fact that (B) was originally bent in a direction orthogonal to the long axis of the R-GAs. This bending released most steric forces, so the R-GAs crystals were relatively stable.

Because the ribbon (B) remained practically intact upon annealing at 500 K, we annealed it at 750 K, as shown in Figure S6. At this high temperature, the ribbon helicity was lost, but its bending was preserved. Upon annealing at 750 K, the ligands became disordered. We can assume that, upon a very slow quenching, the molecules could again attain a crystalline state, but their crystallization into the initial or other configurations would require very slow cooling of the system.

Another interesting situation emerged in (C) and (D), where R-GAs are arranged in rows tilted with respect to the main ribbon axis. Upon annealing, R-GAs undergo a rotational transition into a new phase, especially in (D), where their main axis becomes flipped with respect to the main ribbon axis. Despite this flipping, both ribbons largely retained their original deformation, going mainly along the ribbon axis. All of this behavior illustrates a high level of cooperativity between chiral molecules pinned in crystalline orders to deformable surfaces of limited sizes.

Mixed GA Ribbons

Next, we randomly mixed opposite enantiomers at 3:1 (25S-75R) and 1:1 (50S-50R) ratios in the (A-D) ribbons, as shown in Figures S7 and 4, respectively, and annealed them as in Figure 2 (Methods section). During the preparation of the mixed ribbons, the original R-GAs were randomly replaced by S-GAs, which were attached to the same graphene C atom and adjusted to fit in the space left after the removal of R-GAs. Therefore, until the system is annealed, the mixed structures appear twisted similarly to the homochiral structures, while keeping the memory of the original R-GAs partially replaced by S-GAs. Figure S1 reveals that the calculated forces acting on one S-GA (relaxed) surrounded by 8 R-GAs have more random directions and strengths. As the ratio of opposite enantiomers became similar, the S_2 symmetry was fully lost, which was reflected in the annealed structures. As pointed out earlier, in the racemic systems, the overall torque is canceled. Interestingly, upon annealing, (B) gained the same molecular ordering as the homochiral (B) system in Figure 2, but for a racemic composition. Therefore, the cylindrical deformation of (B) (bending) is preserved, but its helicity is lost, that is, the pitch becomes zero. The other (A, C, D) systems become more random, especially in the racemic state, and their helicity is also lost.

Double GA Ribbons

Finally, we briefly investigated functionalized double graphenes (DGs) formed by two GA-covered graphene ribbons, which were in contact with each other through their free sides. The DGs were formed by (A) or (B) ribbons paired with the same or enantio-opposite ribbons (Methods section). Figure 5a,b shows that when the same enantiomers are present on both sides of DGs, the sheets have the same helicity, they support each other, and DGs are helical. However, since the two sheets have opposite bending, it cancels out in the sandwich. An analogous situation was observed in systems of self-assembled chiral amino acids, which tend to form twisted bilayer ribbons rather than 3D crystals because of uncompensated steric chiral forces.[11,12,15] However, in racemic systems of these amino acids, the chiral forces are compensated; therefore, straight crystals are grown. By analogy, when the two sides of DGs are covered by opposite enantiomers, the sheets have opposite helicities, which cancel each other, so these DGs become flat, as shown in Figure 5c,d. Figures S8 and S9 present additional cases with different rotations and reflections of ribbons.

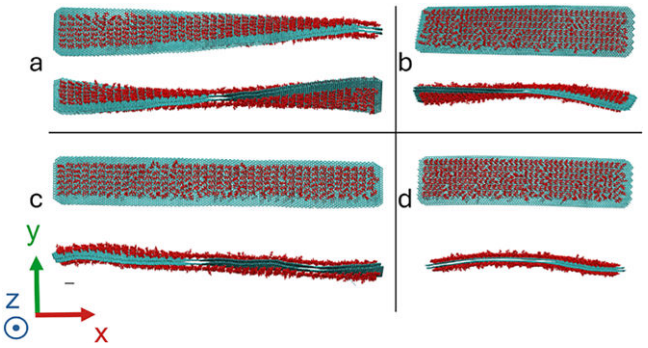

Figure 5. (a) DG A-R/A-R (long axis rotated) system, where both layers are based on A-R ribbons, and the bottom layer is rotated along the long axis. Simulation results in water (t = 118 ns, T = 310 K) show the DG top and side views. (b) Same as (a) for cut B (t = 100 ns). (c) DG A-R/A-L (middle plane reflected) system, where the second GA-graphene layer is a mirror of the top layer in plane between the layers (t = 123 ns). (d) Same as (c) for cut B (t = 100 ns). The scale bar in (c) represents 1 nm.

METHODS

Graphene-based ribbons were constructed with VMD.[43] For simplicity, graphene edges were free, and its C atoms were neutral. GA-R parameters were determined through CHARMM paracheM.[44,45] In the preparation of (25S-75R or 50S-50R) mixed systems, we randomly selected (25 or 50%) GAs, flipped their symmetries, shifted them, and reattached them.

MD simulations were performed with NAMD3[46] and CHARMM36 general force field.[47,48] TIP3P water model was used, and the SHAKE algorithm was used for hydrogens. Nonbonded interactions were evaluated with a switch-off distance of 12 Å. The Velocity Verlet integrator was used to solve the Langevin dynamics with a damping constant of γ_{Lang} = 1 ps^{-1}, and a time step of 2 fs. The simulations were done in the NPT ensemble with periodic boundary conditions applied at different temperatures and a pressure of 1 atm. Particle Mesh Ewald summation[49] was used with a grid spacing of 1 Å. Systems were minimized for 5000 steps. During minimization and pre-equilibration, heavy atoms were constrained, but they were released during the simulations. Data and snapshots were recorded every 10 ps. The 750 K simulations were run in the NVT ensemble without constraints, using a time step of 1 fs, and coordinates were recorded every 5 ps.

The studied intermolecular forces were based on the Coulombic and van der Waals (12−6 Lennard-Jones potential) coupling between the central GA molecule and each of the eight surrounding GAs. These forces were obtained by calculating the change in coupling energies when each ligand is slightly displaced in 3 directions.

CONCLUSIONS

We have simulated model graphene ribbons covered with covalently attached gluconic acid molecules, which were initially organized in a crystalline monolayer. Our simulations

Downloaded from pubs.acs.org/acsodf/article-pdf/11/43/66252/6893534/acsomega.6c04640.pdf by UNIV OF ILLINOIS CHICAGO, Petr Kral on 12 November 2026

https://doi.org/10.1021/acsomega.6c04640
ACS Omega 2026, 11, 66252−66258

of these functionalized ribbons solvated in water have revealed that steric chiral forces acting between R-GAs generate stresses and torques that can bend and helically twist the ribbons in handedness and pitch determined by their crystal structure, enantiomeric excess, and ribbon cut direction. During annealing and quenching, the chiral ligands can gain partly random orientations depending on the temperatures and time sequences used. If the follow-up quenching is slow, then the molecules can crystallize in new structures, with minimal free energies. In the new molecular reorganization, the steric forces acting between the molecules become modified, which causes adjustment of the ribbon geometries. These phenomena should be examined in future experiments to better understand their origin and limits. In such experiments, different molecules might be attached to different flexible substrates, with the molecules exhibiting entirely different organizations. In principle, related deformable nanosystems covered by chiral molecules might respond according to the surrounding conditions and be used in sensing, mimetic, and memory applications.

■ ASSOCIATED CONTENT

Supporting Information

The Supporting Information is available free of charge at https://pubs.acs.org/doi/10.1021/acsomega.6c04640.

Figures of racemic systems, less dense, achiral systems, and their corresponding forces (PDF)

■ AUTHOR INFORMATION

Corresponding Author

Petr Král − *Department of Chemistry, University of Illinois Chicago, Chicago, Illinois 60607, United States; Departments of Physics, Pharmaceutical Sciences, and Chemical Engineering, University of Illinois Chicago, Chicago, Illinois 60607, United States;* orcid.org/0000-0003-2992-9027; Email: pkral@uic.edu

Authors

Pavel L. Rehak − *Department of Chemistry, University of Illinois Chicago, Chicago, Illinois 60607, United States*

Michal Sawczyk − *Department of Chemistry, University of Illinois Chicago, Chicago, Illinois 60607, United States*

Complete contact information is available at: https://pubs.acs.org/10.1021/acsomega.6c04640

Notes

The authors declare no competing financial interest.

■ REFERENCES

(1) Kotov, N. A.; Liz-Marzán, L. M.; Weiss, P. S. Chiral Nanostructures: New Twists. *ACS Nano* **2021**, *15*, 12457−12460.

(2) Visheratina, A.; Kotov, N. A. Inorganic Nanostructures with Strong Chiroptical Activity. *CCS Chem.* **2020**, *2*, 583−604.

(3) Sang, Y.; Liu, M. Hierarchical Self-Assembly into Chiral Nanostructures. *Chem. Sci.* **2022**, *13*, 633−656.

(4) Shimizu, T.; Masuda, M.; Minamikawa, H. Supramolecular Nanotube Architectures Based on Amphiphilic Molecules. *Chem. Rev.* **2005**, *105*, 1401−1443.

(5) Barclay, T. G.; Constantopoulos, K.; Matisons, J. Nanotubes Self-Assembled from Amphiphilic Molecules via Helical Intermediates. *Chem. Rev.* **2014**, *114*, 10217−10291.

(6) Yeom, J.; Yeom, B.; Chan, H.; Smith, K. W.; Dominguez-Medina, S.; Bahng, J. H.; Zhao, G.; Chang, W.-S.; Chang, S.-J.; Chuvilin, A.; Melnikau, D.; Rogach, A. L.; Zhang, P.; Link, S.; Král, P.; Kotov, N. A. Chiral Templating of Self-Assembling Nanostructures by Circularly Polarized Light. *Nat. Mater.* **2015**, *14*, 66.

(7) Yashima, E.; Ousaka, N.; Taura, D.; Shimomura, K.; Ikai, T.; Maeda, K. Supramolecular Helical Systems: Helical Assemblies of Small Molecules, Foldamers, and Polymers with Chiral Amplification and Their Functions. *Chem. Rev.* **2016**, *116*, 13752−13990.

(8) Oda, R.; Huc, I.; Schmutz, M.; Candau, S. J.; MacKintosh, F. C. Tuning Bilayer Twist Using Chiral Counterions. *Nature* **1999**, *399*, 566−569.

(9) Pashuck, E. T.; Stupp, S. I. Direct Observation of Morphological Transformation from Twisted Ribbons into Helical Ribbons. *J. Am. Chem. Soc.* **2010**, *132*, 8819−8821.

(10) Pashuck, E. T.; Cui, H.; Stupp, S. I. Tuning Supramolecular Rigidity of Peptide Fibers through Molecular Structure. *J. Am. Chem. Soc.* **2010**, *132*, 6041−6046.

(11) Shaham-Niv, S.; Rehak, P.; Vuković, L.; Alder-Ambramovich, L.; Král, P.; Gazit, E. Formation of Aptosis-inducing Amyloid Fibrils by Tryptophan. *Isr. J. Chem.* **2017**, *57*, 729−737.

(12) Bera, S.; Xue, B.; Rehak, P.; Jacoby, G.; Ji, W.; Shimon, L. J. W.; Beck, R.; Král, P.; Cao, Y.; Gazit, E. Self-Assembly of Aromatic Amino Acid Enantiomers into Supramolecular Materials of High Rigidty. *ACS Nano* **2020**, *14*, 1694−1706.

(13) Cho, K. R.; Salter, E. A.; De Yoreo, J. J.; Wierzbicki, A.; Elhadj, S.; Huang, Y.; Qiu, S. R. Impact of Chiral Molecules on the Formation of Biominerals: A Calcium Oxalate Monohydrate Example. *Cryst. Growth Des.* **2012**, *12*, 5939−5947.

(14) Weissbuch, I.; Leiserowtiz, L.; Lahav, M. Molecular recognition in chiral and non-chiral amphiphilic self-assemblies at interfaces. *Curr. Opin. Colloid Interface Sci.* **2008**, *13*, 12−22.

(15) Rehak, P.; Král, P. Hybridization of Biomolecular Crystals and Low-Dimensional Materials. *ACS Nano* **2021**, *15*, 6678−6683.

(16) Pranav; Ghali, E. N. H. K.; Chauhan, N.; Tiwari, R.; Cabrera, M.; Chauhan, S. C.; Yallapu, M. M. One-step simultaneous liquid phase exfoliation-induced chirality in graphene and their chirality-mediated microRNA delivery. *Mater. Adv.* **2023**, *4*, 6199−6212.

(17) Singh, G.; Chan, H.; Baskin, A.; Gelman, E.; Repnin, N.; Král, P.; Klajn, R. Self-Assembly of Magnetite Nanocubes into Helical Superstructures. *Science* **2014**, *345*, 1149.

(18) Jana, S.; de Frutos, M.; Davidson, P.; Abécassis, B. Ligand-Induced Twisting of Nanoplatelets and Their Self-Assembly into Chiral Ribbons. *Sci. Adv.* **2017**, *3*, No. e1701483.

(19) Monego, D.; Dutta, S.; Grossman, D.; et al. Ligand-Induced Incompatible Curvatures Control Ultrathin Nanoplatelet Self-Assembly. *Proc. Natl. Acad. Sci. U.S.A.* **2024**, *121*, No. e2316299121, DOI: 10.1073/pnas.2316299121.

(20) Guillemeney, L.; Lermusiaux, L.; Landaburu, G.; et al. Curvature and Self-Assembly of Semiconducting Nanoplatelets. *Commun. Chem.* **2022**, *5*, No. 7.

(21) Lee, H.-E.; Kim, R. M.; Ahn, H. Y.; et al. Cysteine-Encoded Chirality Evolution in Plasmonic Rhombic Dodecahedral Gold Nanoparticles. *Nat. Commun.* **2020**, *11*, No. 263.

(22) Häkkinen, H. The Gold-Sulfur Interface at the Nanoscale. *Nat. Chem.* **2012**, *4*, 443−455.

(23) Dong, J.; Liu, Y.; Cui, Y. Emerging Chiral Two-Dimensional Materials. *Nat. Chem.* **2024**, *16*, 1398−1407.

(24) Zheng, J.; Boukouvala, C.; Lewis, G. R.; Ma, Y.; Chen, Y.; Ringe, E.; Shao, L.; Huang, Z.; Wang, J. Halide-Assisted Differential Growth of Chiral Nanoparticles with Threefold Rotational Symmetry. *Nat. Commun.* **2023**, *14*, No. 3783.

(25) Wang, P.-p.; Yu, S.-J.; Govorov, A. O.; Ouyang, M. Cooperative Expression of Atomic Chirality in Inorganic Nanostructures. *Nat. Commun.* **2017**, *8*, No. 14312.

(26) Lee, H.-E.; Ahn, H.-Y.; Mun, J.; Lee, Y. Y.; Kim, M.; Cho, N. H.; Chang, K.; Kim, W. S.; Rho, J.; Nam, K. T. Amino-acid- and peptide-directed synthesis of chiral plasmonic gold nanoparticles. *Nature* **2018**, *556*, 360.

Downloaded from pubs.acs.org/acsodf/article-pdf/11/43/66252/6893534/acsomega.6c04640.pdf by UNIV OF ILLINOIS CHICAGO, Petr Kral on 12 November 2026

(27) Ni, B.; Mychinko, M.; Gómez-Graña, S.; Morales-Vidal, J.; Obelleiro-Liz, M.; Heyvaert, W.; Vila- Liarte, D.; Zhuo, X.; Albrecht, W.; Zheng, G.; González-Rubio, G.; Taboada, J. M.; Obelleiro, F.; López, N.; Pérez-Juste, J.; Pastoriza-Santos, I.; Cölfen, H.; Bals, S.; Liz-Marzán, L. M. Chiral Seeded Growth of Gold Nanorods Into Fourfold Twisted Nanoparticles with Plasmonic Optical Activity. *Adv. Mater.* **2023**, *35*, No. 2208299.
(28) Bi, Y.; Cheng, C.; Zhang, Z.; Liu, R.; Wei, J.; Yang, Z. Controlled Hierarchical Self-Assembly of Nanoparticles and Chiral Molecular into Tubular Nanocomposites. *J. Am. Chem. Soc.* **2023**, *145*, 8529−8539.
(29) González-Rubio, G.; Mosquera, J.; Kumar, V.; Pedrazo-Tardajos, A.; Llombart, P.; Solís, D. M.; Lobato, I.; Noya, E. G.; Guerrero-Martínez, A.; Taboada, J. M.; Obelleiro, F.; MacDowell, L. G.; Bals, S.; Liz- Marzán, L. M. Micelle-directed chiral seeded growth on anisotropic gold nanocrystals. *Science* **2020**, *368*, 1472.
(30) Love, J. C.; Estroff, L. A.; Kriebel, J. K.; Nuzzo, R. G.; Whitesides, G. M. Self-Assembled Monolayers of Thiolates on Metals as a Form of Nanotechnology. *Chem. Rev.* **2005**, *105*, 1103−1169.
(31) Heuer-Jungemann, A.; Feliu, N.; Bakaimi, I.; et al. The Role of Ligands in the Chemical Synthesis and Applications of Inorganic Nanoparticles. *Chem. Rev.* **2019**, *119*, 4819−4880.
(32) Lee, C.; Wei, X.; Kysar, J. W.; Hone, J. Measurement of the Elastic Properties and Intrinsic Strength of Monolayer Graphene. *Science* **2008**, *321*, 385−388.
(33) Lindahl, N.; Midtvedt, D.; Svensson, J.; et al. Determination of the Bending Rigidity of Graphene via Electrostatic Actuation of Buckled Membranes. *Nano Lett.* **2012**, *12*, 3526−3531.
(34) Blees, M. K.; Barnard, A. W.; Rose, P. A.; et al. Graphene Kirigami. *Nature* **2015**, *524*, 204−207.
(35) Ma, S.; Gu, J.; Lin, C.; et al. Supertwistacene: A Helical Graphene Nanoribbon. *J. Am. Chem. Soc.* **2020**, *142*, 16887−16893.
(36) Chamberlain, T. W.; Biskupek, J.; Rance, G. A.; et al. Size, Structure, and Helical Twist of Graphene Nanoribbons Controlled by Confinement in Carbon Nanotubes. *ACS Nano* **2012**, *6*, 3943−3953.
(37) Dontsova, E.; Dumitrică, T. Nanomechanics of Twisted Mono- and Few-Layer Graphene Nanoribbons. *J. Phys. Chem. Lett.* **2013**, *4*, 2010−2014.
(38) Song, M.; Tong, L.; Liu, S.; et al. Nonlinear Amplification of Chirality in Self-Assembled Plasmonic Nanostructures. *ACS Nano* **2021**, *15*, 4160−4171.
(39) Wang, Y.; Qi, W.; Huang, R.; et al. Rational Design of Chiral Nanostructures from Self-Assembly of a Ferrocene-Modified Dipeptide. *J. Am. Chem. Soc.* **2015**, *137*, 7869−7880.
(40) Huang, Y.; Wei, X. Self-Assembly of Chiral Amphiphiles with π-Conjugated Tectons. *Sci. China Life Sci.* **2012**, *57*, 4246−4256.
(41) Savin, A. V.; Korznikova, E. A.; Kivshar, Y. S. Twistons in Graphene Nanoribbons on a Substrate. *Phys. Rev. B* **2020**, *102*, No. 245432.
(42) Fonseca, A. F. Twisting or Untwisting Graphene Twisted Nanoribbons without Rotation. *Phys. Rev. B* **2021**, *104*, No. 045401.
(43) Humphrey, W.; Dalke, A.; Schulten, K. VMD: Visual Molecular Dynamics. *J. Mol. Graphics* **1996**, *14*, 33−38.
(44) Vanommeslaeghe, K.; Mackerell, A. D. Automation of the CHARMM General Force Field (CGenFF) I: Bond Perception and Atom Typing. *J. Chem. Inf. Model.* **2012**, *52*, 3144−3154.
(45) Vanommeslaeghe, K.; Raman, E. P.; Mackerell, A. D. Automation of the CHARMM General Force Field (CGenFF) II: Assignment of Bonded Parameters and Partial Atomic Charges. *J. Chem. Inf. Model.* **2012**, *52*, 3155−3168.
(46) Phillips, J. C.; Braun, R.; Wang, W.; Gumbart, J.; Tajkhorshid, E.; Villa, E.; Chipot, C.; Skeel, R. D.; Kalé, L.; Schilten, K. Scaleable Molecular Dynamics with NAMD. *J. Comput. Chem.* **2005**, *26*, 1781−1802.
(47) Vanommeslaeghe, K.; Hatcher, E.; Acharya, C.; et al. CHARMM General Force Field: A Force field for Drug-Like Molecules Compatible with the CHARMM All-Atom Additive Biological Force Field. *J. Comput. Chem.* **2010**, *31*, 671−690.
(48) Yu, W.; He, K.; Vanommeslaeghe, K.; Mackerell, A. D. Extension of the CHARMM General Force Field to Sulfonyl-Containing Compounds and Its Utility in Biomolecular Simulations. *J. Comput. Chem.* **2012**, *33*, 2451−2468.
(49) Darden, T.; York, D.; Pedersen, L. Particle Mesh Ewald: An n·log(n) Method for Ewald Sums in Large Systems. *Chem. Phys.* **1993**, *98*, 10089−10092.

Downloaded from pubs.acs.org/acsodf/article-pdf/11/43/66252/6893534/acsomega.6c04640.pdf by UNIV OF ILLINOIS CHICAGO, Petr Kral on 12 November 2026

https://doi.org/10.1021/acsomega.6c04640
ACS Omega 2026, 11, 66252−66258